3D CONSTRAINED LOCAL MODEL WITH INDEPENDENT COMPONENT ANALYSIS AND NON-GAUSSIAN SHAPE PRIOR DISTRIBUTION: APPLICATION TO 3D FACIAL LANDMARK DETECTION

Marwa C. El Rai[⋆]*, Claudio Tortorici*[⋆]*, Hassan Al-Muhairi*[⋆]*, Marius George Linguraru*[†]*, Naoufel Werghi*[⋆]

[⋆]Khalifa University, UAE [†]Children's National Health System, USA

ABSTRACT

We present a novel statistical shape model and fitting process for the 3D Constrained Local Models (CLM), exploiting the properties of Independent Component Analysis (ICA), instead of the classic use of Principal Component Analysis (PCA), and adopting a non-Gaussian distribution of the shape prior information. Using ICA permits to exploit the real distribution of shape priors by adopting a Generalised Gaussian Distribution (GGD) model. Consequently, we derive a modified approach of the mean shift optimizer by using the Expectation-Maximization algorithms. We apply this novel method for the localization of face landmarks on 3D facial mesh models, which, to the best of our knowledge, is the first employment of the CLM variant on this kind of modality. Experiments conduced on the Bosphorus face database demonstrated that our approach outperforms state-of-the-art methods.

Index Terms— CLM, ICA, Mesh-LBP, Gaussian Generalized Distribution, Facial Landmarks detection.

1. INTRODUCTION AND RELATED WORK

Statistical shape model (SSM) is a popular computer vision technique able to localize landmarks pre-defined over the object of interest. SSM can be applied to faces, organs, human bodies, or general geometric objects. The subject has been studied for decades, from the classic active shape model [1] and active appearance model [2] to the more recently proposed constrained local model (CLM) [3]. It has been deployed in many successful applications, such as face alignment, expression recognition, and general medical image analysis.The differences between various SSM methods mainly lay in the statistical techniques used for the training, optimization strategies used for fitting, and approaches used to model the object's appearance. Despite the large amount of work devoted to improve the performance of SSM, increasing the accuracy and robustness of such models remains an important motivation, especially for applications that require very high precision. For example, the recognition of facial expression and dysmorphology would benefit from better landmark detection because the difference between various instances is often geometrically very subtle. We provided such as example in our pilot study targeting Down syndrome detection using 3D face scans and based on facial landmark analysis using SSM [4, 5]. To the best of our knowledge, there is no previous work related to the CLM on mesh models. The CLM-Z framework, operating on depth images, was used by Baltruatis et al [6] and Cheng et al [7]. It requires pose normalization and suffers from the loss of the shape information because of the 2D projections. The authors in [6, 7] also used PCA and Gaussian shape priors for their SSM. On the other hand, some researchers proposed methods for 3D landmarking by exploiting directly the mesh data. Here, we present the most recent and competitive methods adopting a similar experimental close to ours. A comprehensive survey can be found in [8, 9, 10]. Creusot et al. [10] proposed a landmark localization method based on shape information and keypoint concept. Typically, many keypoint candidates are identified on a local 3D mesh and the most probable candidates are identified through shape analysis. Driven by robustness to occlusion, Sukno et al. [8] proposed an RANSAC-based matching of an SSM to candidate points generated via asymmetry patterns shape contexts. The SSM was build via PCA and assuming Gaussian shape priors. Gamgoz et al. [9] suggested a supervised descent method (SDM) optimization framework employing a ridge regression learning. While the approach is elegantly implemented, the update of the landmark vector during the optimization is hard to implement on the mesh manifold. This limits the method's application to the depth image assuming frontal pose (e.g. no rotation and no occlusions). In this paper, we propose a novel CLM framework adapted for mesh manifolds and showcase its merit on face mesh landmark detection in the presence of deformations, occlusions and missing parts. Our original contribution is two-fold: first, we employ ICA [11] to model shape variation rather than PCA; second, we propose a CLM implementation on 3D facial triangular mesh models. To the best of our knowledge all CLM-based landmark face detection methods, including the recent variant of Baltrusaitis et al. [6], operate only on depth images. Our motivation is that PCA-based models assume a Gaussian distribution of shape variations, which is often invalid, especially when working with complex shapes. In addition, the bases of PCA tend to

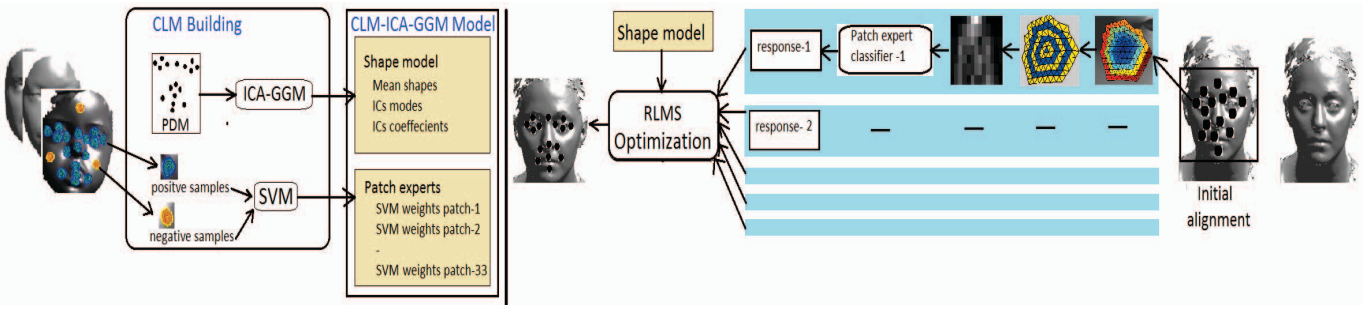

Fig. 1. Framework of CLM-ICA-GGD applied to facial landmark detection for the 3D face mesh models. From a training set of 100 3D scans we manually select a set 33 face landmark from each scan. These are fed into the ICA analysis considering a GGD shape priors to build our SSM. Descriptors extracted from training landmarks neighbourhood (positive samples) and from different regions (negative samples) are used to build the patch model, that is an SVM-based classifier. The outcome is a shape model and patch experts that describe, respectively, the global face shape variation, and the local variation around each landmark. Testing: After a first rough alignment of the shape model on face scan, an ordered neighborhood is constructed[12], around each initial landmark estimate, and from which we build 2D Histograms derived from mesh-LBP desriptors [13, 14, 15]. These histograms are the input of the patch experts. The landmarks detection is performed using constrained optimization that searches for the landmark positions that maximizes the patch expert responses while fitting the shape model.

represent only the global shape variations. We introduce a novel CLM fitting algorithm that model not only the response map, but also the shape prior by non-Gaussian probability distributions, namely a Generalized Gaussian Distribution, to be consistent with the intrinsic non-Gaussianity of ICA. This CLM implementation is facilitated by the use of an ordered and structured neighborhood on the mesh [12]. Our method addresses the need of pose normalization while preserving the full geometry of the facial surface, which is not the case in depth images because of the orthogonal projection. Fig. 1 summarizes the structure and the stages of our framework.

2. THE CLM-ICA-GGD APPROACH

Given a triangle mesh face model $M(\mathbf{f}, \mathbf{v})$ defined by the sets of facets **f** and vertices **v**, we define a CLM model composed of a deformable shape model and a patch model describing both global and local morphology. Our shape model is represented by a Point Distribution Model (PDM) [16], namely, the coordinates of n landmark points $\mathbf{V} = (x_1, y_1, z_1, ..., x_n, y_n, z_n)^t$, described by:

$$\mathbf{V}(\mathbf{p}) = s\mathbf{R}(\bar{\mathbf{V}} + \Phi\mathbf{q}) + \mathbf{t}, \tag{1}$$

where $\bar{\mathbf{V}}$ is the mean shape model. The shape is controlled by the *m* components of linear deformation, described using the $n \times m$ basis matrix Φ, and the set of model parameters $\mathbf{p} = [\mathbf{s}, \mathbf{R}, \mathbf{t}, \mathbf{q}]$ that includes the scaling factor **s**, rotation **R**, translation **t**, and the vector **q**, which reveals the non-rigid variation of the shape. All the training instances of **V**, are aligned and normalized via Procrustes analysis. In the case of PCA, Φ represents an orthogonal basis composed of eigen vectors. In the case of ICA, we build the SSM $\mathbf{V} = \mathbf{A}.\mathbf{S}$, where **V** and **S** denote the shape matrix and column matrix of the Independent Components (ICs), respectively. ICA represents a class of algorithms that seek a linear transformation **W** that maximizes the statistical independence of **S = W.V**. The linear transform **W** is defined as an inverse of the basis matrix, $\mathbf{W} = \mathbf{A}^{-1}.\mathbf{X}$, and is called de-mixing matrix. ICA is known to produce more spatially localized basis vectors than PCA, facilitated by its kurtosis optimization, which maximizes the non-Gaussianity in ICs [17]. Exploiting this merit, ICA can represent the shape subspace Φ in the PDM model equation (1). In this case, Φ is the sub-matrix of the ICA basis matrix **A** called mixing matrix. For the sake of simplicity, usually the probability associated with a shape defined by parameters **q** is assumed to be a normal distribution. In our approach, we use GGD which has a larger probability density registration [18]. The GGD will be described in section 2.1.

The patch expert is a linear classifiers, $P = [w_j, b_j]$, associated to the j^{th} landmark, where w_j and b_j are the weights and bias parameters. It is trained for each facial landmark using positive and negative samples selected from training data using a linear Support Vector Machine (SVM) [18] due to its computational advantage and discriminating power. Let $l_j \in \{-1, 1\}$ be a discrete random variable, which indicates if the j^{th} landmark is aligned or misaligned. The response map, which is defined as the probability for the j^{th} landmark being correctly aligned $(l_j = 1)$ at vertex **v** of mesh *M*, is normalized by a sigmoid function providing an estimate of the likelihood of the landmark's alignment [3]:

$$p(l_j = 1/v, M) = \frac{1}{1 + e^{-(w_j^T C(\mathbf{v};M) + b_j)}} \tag{2}$$

$C(\mathbf{v}; M)$ denotes he 2D histograms constructed from the mesh-LBP descriptors [13, 14, 15] that are computed on the mesh surface at an ordered and structured neighborhood [12] around the vertex **v**.

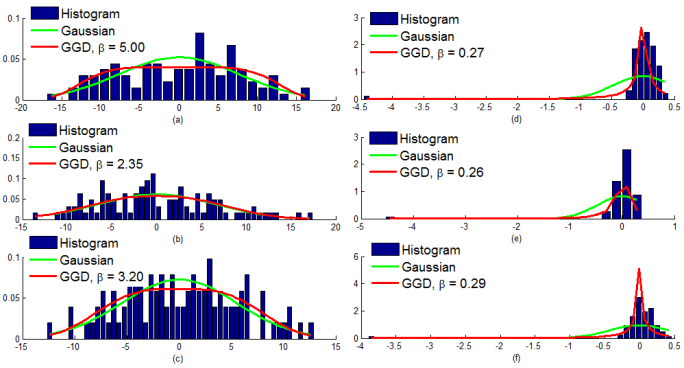

Fig. 2. Histograms and the probability density of Gaussian and GGD distributions for the first three modes obtained by PCA (left from top (a) p=0.30, (b) p=0.90, (c) p=0.90) and and ICA (right from top (d) $p < 0.001$, (e) $p < 0.001$ and (f) $p < 0.001$)

2.1. CLM fitting with GGD shape prior

The CLM's shape prior in the function (1) is considered to follow a GGD model in our proposed method. Consequently, the fitting algorithm regularized landmark mean shift (RLMS) [3] in the general framework (see figure 1) should be updated according to the new SSM. Note that the shape prior is used to model the non-rigid shape variations, while the rigid part of the shape prior is assumed to be uniform. The m-dimensional GGD is defined as [19]:

$$p(\mathbf{q};\mu,\beta,\Sigma) = \frac{[det(\Sigma)]^{-2}}{[Z(\beta)A(\beta)]^{D}} e^{-\left(\|\frac{\Sigma^{-1/2}(\mathbf{q}-\mu)}{A(\beta)}\|_{\beta}\right)}, \quad (3)$$

where β is the shape parameter, μ represents the mean of the distribution, and Σ is an asymmetric positive definite matrix. $\Gamma(.)$ is the Gamma function i.e. $\Gamma(z) = \int_0^{\infty} e^{-t}t^{z-1}dt$, $Z(\beta) = \frac{2}{\beta}\Gamma\left(\frac{1}{\beta}\right)$ and $A(\beta) = \sqrt{\frac{\Gamma(1/\beta)}{\Gamma(3/\beta)}}$ is referred to as the scale parameter. $\|\mathbf{q}\|_{\beta} = \sum_{i=1}^{D}|q_i|^{\beta}$ stands for the l_{β} norm of vector $\mathbf{q}$. By inferring β, a wide class of statistical distributions can be characterized including uniform, Gaussian, Laplacian, and other sub-band super-Gaussian densities. We estimate the GGD parameters $\pi = (\mu, \beta, \Sigma)$ from a set of 100 training shapes $\{\mathbf{q}_1, ...\mathbf{q}_N\}$ assumed to be independently and identically distributed using the the maximum-likelihood estimator [20]. Fig. 2 depicts the shape parameter distributions of the first three modes obtained by PCA and ICA modeled by using Gaussian and GGD, and obtained from the training set. Significance is computed by the Chi-square goodness-of-fit test. If $p < 0.05$, the data do not follow a normal distribution. We can notice that the Gaussian and GGD generate close estimations in the case of PCA, whereas in the case of ICA a non-Gaussian distribution is obtained as it is confirmed by the goodness of fit test.

Under the probabilistic formulation of CLM, the fitting algorithm looks for the maximum *a posteriori* probability of the deformable model parameters $\mathbf{p}$ [3, 6]:

$$p(\mathbf{p}|\{l_j = 1\}_{j=1}^{n}, M) \propto p(\mathbf{p}) \prod_{j=1}^{n} p(l_j = 1/\mathbf{v}_j, M\}, \quad (4)$$

where $p(\mathbf{p})$ is the prior probability of the model parameters $\mathbf{p}$ assumed to be a GGD. Consequently, we adapt this GDD prior to the RLMS framework that aims to estimate and update the PDM parameters $\mathbf{p}$ that jointly minimizes the misalignment error over all landmarks. The optimization of the function (4) is carried out using the Expectation Maximization (EM) algorithm. In RLMS, the E step models the response map $p(l_j = 1/\mathbf{v}_j, M)$ as kernel density estimator with bandwidth ρ. We derive the M-step by minimizing the expectation of the negative-log of the complete likelihood by Newton's method as follows:

$$\Im(\mathbf{p}) = E\left[-ln\left(p(\mathbf{p})\Pi_{j=1}^{n} p(l_j = 1 \mid \mathbf{v}_j, M)\right)\right] \quad (5)$$

The gradient vector $\mathbf{g}_{GDD}(\mathbf{p})$ of the objective $\Im(\mathbf{p})$ is given by:

$$\begin{aligned}\mathbf{g}_{GGD}(\mathbf{p}) &= \nabla_{\mathbf{p}}\Im\mathbf{p} = \nabla_{\mathbf{q}}\Im\mathbf{q} \\ &= \frac{\beta\Sigma^{-1/2}}{A(\beta)}\left(\|\frac{\Sigma^{-1/2}(\mathbf{q}-\mu)}{A(\beta)}\|_{\beta-1}\right) - \frac{1}{\rho}\mathbf{J}^T\mathbf{m},\end{aligned}$$

where $\mathbf{m} = (m_1, m_2, ..., m_n)^t$ is the mean shift vector defined over the landmarks which are projected to a subspace spanned by the Jacobian $\mathbf{J}$ of the PDM [3]. The Hessian matrix of $\Im(\mathbf{p})$ is then given by:

$$\begin{aligned}\mathbf{H}_{GGD}(\mathbf{p}) &= \nabla^2_{\mathbf{p}}\Im\mathbf{p} = \nabla^2_{\mathbf{q}}\Im\mathbf{q} \\ = \beta(\beta-1)\left(\frac{\Sigma^{-1/2}}{A(\beta)}\right)^2&\left(\|\frac{\Sigma^{-1/2}(\mathbf{q}-\mu)}{A(\beta)}\|_{\beta-2}\right) - \frac{1}{\rho}\mathbf{J}^T\mathbf{J}\end{aligned}$$

Finally, the update rule of the shape parameters for the M-step with the proposed GGD shape prior is given by:

$$\Delta\mathbf{p} = -\mathbf{H}_{GGD}(\mathbf{p})^{-1}\mathbf{g}_{GGD}(\mathbf{p}) \quad (6)$$

	PCA	ICA-Gaussian	ICA-GGD
Mean curvature	2.84 ± 1.49	2.81 ± 1.49	$\mathbf{2.71 \pm 1.29}$
Curvedness	2.80 ± 1.46	2.78 ± 1.46	$\mathbf{2.75 \pm 1.29}$

Table 1. Comparison of the mean landmark localization error obtained using PCA, ICA-Gaussian and our proposed ICA-GCD.

3. EXPERIMENTS

We conducted two series of experiments that aim at: 1) demonstrating the superiority of the CLM-ICA-GGD framework over the standard PCA assuming Guassian shape priors, and 2) comparing the performance of our method against state of the art facial landmark detection methods. We used the Bosphorus database [21], which contains 4666 scans of 105 subjects scanned in different poses, expressions and occlusion conditions. Each sample contains 24 facial landmark

(a)

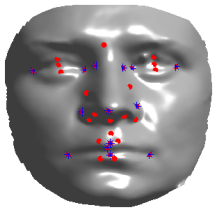

(b)

	[10]	[8]	[9]	Our method
LM	14	14	22	33
Training size	99	99	1420x2	100
Test size	2803	2902	1420x2	4230
Features	key points	APSC	HOG	mesh-LBP[13]
Technique	LDA-Adaboost	Shape-regression-Ransac	SDM-SRD	CLM-ICA-GGD

(c)

ID	Creusot et al. [10]	Sukno et al. [8]	Camgoz et al. [9]	ICA-GGD (this paper)
1	6.04 ± 3.85	4.87 ± 3.54	4.87 ± 1.45	**2.45 ± 1.93**
2	3.92 ± 2.54	2.69 ± 1.93	**1.9 ± 2.30**	2.48 ± 1.56
3	3.95 ± 2.65	2.82 ± 2.04	**1.84 ± 3.20**	2.39 ± 1.32
4	6.15 ± 4.08	5.14 ± 3.79	**2.51 ± 2.55**	2.78 ± 1.35
5	-	-	6.78 ± 3.59	**3.03 ± 2.05**
6	-	-	6.92 ± 3.66	**4.57 ± 3.89**
7	10.08 ± 3.44	8.88 ± 3.48	1.96 ± 1.20	**1.76 ± 1.50**
8	5.02 ± 2.84	3.17 ± 2.11	2.65 ± 2.76	**2.19 ± 1.89**
9	5.90 ± 4.09	8.95 ± 4.04	1.99 ± 3.17	**1.53 ± 2.65**
10	7.95 ± 5.43	5.94 ± 5.08	2.92 ± 2.13	**1.57 ± 1.89**
11	5.28 ± 3.54	3.92 ± 2.91	**2.46 ± 2.04**	3.00 ± 2.50
12	7.60 ± 5.41	6.02 ± 5.10	2.91 ± 2.07	**2.45 ± 3.05**
13	6.79 ± 2.50	-	**2.39 ± 1.96**	2.50 ± 2.89
14	-	-	**2.39 ± 2.28**	2.50 ± 2.88

(d)

ID	Creusot et al. [10]	Sukno et al. [8]	ICA-GGD (this paper)
1	6.79 ± 6.90	5.57 ± 6.53	**3.98 ± 2.74**
2	4.58 ± 5.13	3.53 ± 4.35	**2.98 ± 2.72**
3	4.10 ± 4.69	**2.93 ± 2.07**	3.22 ± 2.15
4	6.50 ± 7.54	**5.27 ± 4.93**	6.07 ± 4.86
7	10.24 ± 4.13	9.31 ± 5.43	**5.61 ± 3.82**
8	4.95 ± 3.38	3.64 ± 4.18	**2.55 ± 1.45**
9	8.46 ± 4.19	7.55 ± 4.84	**5.80 ± 3.04**
10	5.35 ± 5.15	4.18 ± 7.32	**3.48 ± 2.89**
11	3.98 ± 3.16	**3.18 ± 5.54**	3.50 ± 2.52
12	4.84 ± 4.68	**4.12 ± 6.21**	4.50 ± 3.63

Table 2. (a):Sample face from the Bosphorus database showing the 33 landmarks used to train the facial model and 14 annotated landmarks. (b):Main features and experimental setup of the compared methods. (c): Mean ± stdev associated with each of the automatically localized landmarks of the frontal facial scans for the compared methods. 1: Outer left eye corner. 2: Inner left eye corner. 3: Inner right eye corner. 4: Outer right eye corner. 5: Nose saddle left. 6: Nose saddle right. 7: Left corner of nose. 8: Nose tip. 9: Right corner of nose. 10: Left mouth corner. 11: Upper lip outer middle. 12: Right mouth corner. 13: Upper lip inner middle. 14: Lower lip inner middle. (d):Mean/stdev obtained for the group of face scans rotated and under occlusions.

positions manually annotated. Our PDM includes 33 landmarks but only 14 of them are part of the ground truth set provide by the Bosphorus database (Tab.2.a). Therefore we used these to evaluate and compare our method with the other ones. The set of face scans we used in the testing includes frontal, expressions rotated and occluded instances. We compared our approach with the methods proposed in [10, 8, 9] that used the same database and adopted an experimental setting close to ours. [10, 8] reported their detected landmarks online. In all the experiments, the errors were computed as the Euclidean distance between the automatically localized and the corresponding ground truth landmarks. Tab.1 depicts the mean/stdev of the landmark localization error defined as the absolute distance between the estimated and the ground truth landmark locations, obtained with the PCA, ICA with Gaussian priors, and two variants of our method using mesh-LBP computed with mean curvature and the curvedness. Tab.2.b summarizes the main features of these methods together with our method. Tab.2.c and Tab.2.d report, respectively, the localization error obtained for the group of the frontal scans, and the group including rotated and occluded scans, respectively, for each landmark. For the first group, we can notice that our approach outperforms the methods of [10] and [8] while it compares well with [9]. For the second group we can see that our method outperforms [10] and scores better than [8] at many instances. The method [9] does not report results to include in Table 2.d as it is applicable only to frontal scans.

4. CONCLUSION

In this paper, we have introduced a general ICA-based CLM method with non-Gaussian shape prior applied to the detection of the 3D facial landmarks. The shape prior in model fitting was estimated using a Generalized Gaussian Distribution. The method was applied to facial landmark detection in datasets with complex shape variability. The comparison with static shape model distributions adopting PCA and assuming Gaussian shape priors evidenced the limitation of this model in holding complex shape variations. The results also indicates that the Gaussian distribution is not accurate to model the shape prior obtained by ICA and may degrade the performance of the model. Applied to 3D face landmark detection, our SSM approach exhibits a robust performance, competing and even outperforming state-of-the-art methods. While the comparison is not comprehensive it gives a strong indication of the potential of our SSM approach for addressing complex and non-linear deformable shape modeling problems. In the future work, we will investigate other shape priors, such as non-parametric shape priors and shape priors suited to 2D manifolds (e.g.diffusion maps [22]).

5. REFERENCES

[1] T. F. Cootes and C. J. Taylor, "Active shape models smart snakes," in *BMVC 92*, 1992, pp. 266–275.

[2] T. Cootes, G. Edwards, and C. Taylor, "Active appearance models," in *ECCV'98*, 1998, pp. 448–498.

[3] J. Saragih, S. Lucey, and J. Cohn, "Deformable model fitting by regularized landmark mean-shift," *Int. Journal of Computer Vision*, vol. 91, pp. 200–215, 2011.

[4] Q. Zhao, K. Okada, K. Rosenbaum, L. Kehoe, DJ. Zand R. Sze, M. Summar, and M. Linguraru, "Digital facial dysmorphology for genetic screening: Hierarchical constrained local model using ica," *Medical Imge Analysis*, vol. 18, pp. 699–710, 2014.

[5] M. Chendeb et al, "Landmark detection from 3d mesh facial models for image-based analysis of dysmorphology," in *EMBC'2015*. IEEE, 2015, pp. 169–172.

[6] T. Baltruaitis, P. Robinson, and L.P. Morency, "3d constrained local model for rigid and non-rigid facial tracking," *IEEE Computer Vision and Pattern Recognition*, 2012.

[7] Sh. Cheng, S. Zafeiriou, A. Asthana, and M. Pantic, "3d facial geometric features for constrained local model," *IEEE International Conference on Image Processing*, October 2014.

[8] F. M. Sukno, J. L. Waddington, and P. F. Whelan, "3-d facial landmark localization with asymmetry patterns and shape regression from incomplete local features," *IEEE Trans. Systems, Men and Cybernetics*, vol. 45, no. 9, pp. 1717–1730, 2015.

[9] N. Camgoz, V. struc, B. Gokberk, L. Akarun, and A. Kindiroglu, "Facial landmark localization in depth images using supervised ridge descent," in *ICCV workshops*, 2015, pp. 136–141.

[10] C. Creusot, N. Pears, and J. Austin, "A machine-learning approach to keypoint detection and landmarking on 3d meshes," *International journal of computer vision*, vol. 102, no. 3, pp. 146–179, 2013.

[11] P. Comon, "Independent component analysis, a new concept?," in *Signal Processing*, 1994, vol. 36, pp. 287–314.

[12] N. Werghi, M. Rahayem, and J. Kjellander, "An ordered topological representation of 3d triangular mesh facial surface: concept and applicationss," *EURASIP Journal on Advances in Signal Processing*, vol. 139, pp. 144–159, 2012.

[13] N. Werghi, S. Berretti, and A. del Bimbo, "The mesh-lbp: a framework for extracting local binary patterns from discrete manifolds," *Computer Vision and Image Understanding*, vol. 139, pp. 161–177, 2015.

[14] N. Werghi, C. Tortorici, S. Berretti, and A. del Bimbo, "Local binary patterns on triangular meshes: Concept and applications," *IEEE Transactions on Image Processing*, vol. 24, no. 1, pp. 220–235, 2015.

[15] N. Werghi, C. Tortorici, S. Berretti, and A. del Bimbo, "Representing 3d texture on mesh manifolds for retrieval and recognition applications," in *CVPR'2015*, pp. 2521–2530.

[16] T.F. Cootes and C.J. Taylor, "Statistical models of appearance for computer vision," 2004.

[17] Anthony J Bell and Terrence J Sejnowski, "The independent components of natural scenes are edge filters," *Vision research*, vol. 37, no. 23, pp. 3327–3338, 1997.

[18] S. Nadarajah, "A generalized normal distribution," *Journal of Applied Statistics*, vol. 32, no. 7, pp. 685–694, 2005.

[19] Manuele Bicego, Daniel Gonzalez-Jimenez, Enrico Grosso, and JL Alba Castro, "Generalized gaussian distributions for sequential data classification," in *Pattern Recognition, 2008. ICPR 2008. 19th International Conference on*. IEEE, 2008, pp. 1–4.

[20] M.N. Do and M. Vetterli, "Wavelet-based texture retrieval using generalized gaussian density and kullback-leibler distance," *Image Processing, IEEE Transactions on*, vol. 11, no. 2, pp. 146–158, Feb 2002.

[21] N. Alyz, B. Gkberk, and L. Akarun, "3D face recognition system for expression and occlusion invariance," in *IEEE Int. Conf. on Biometrics: theory, applications, and systems*, Washington, DC, USA, 2008, pp. 1–7.

[22] N. Thorstensen, P. Etyngier, F. Segonne, and R. Keriven, "Diffusion maps as a framework for shape modeling," *Computer Vision and Image Understanding*, vol. 115, no. 4, pp. 520–530, 2011.